

Electrodeposition of $\text{Bi}_{1-x}\text{Sb}_x$ Films and 200-nm Wire Arrays from a Nonaqueous Solvent

Marisol Martín-González,^{*,†} Amy L. Prieto,^{†,§} Meredith S. Knox,[†]
Ronald Gronsky,[‡] Timothy Sands,^{‡,||} and Angelica M. Stacy[†]

Department of Chemistry and Department of Materials Science and Engineering,
University of California—Berkeley, Berkeley, California, 94720

Received October 17, 2002. Revised Manuscript Received January 28, 2003

Films and 200-nm wire arrays of $\text{Bi}_{1-x}\text{Sb}_x$ alloys, one of the best known low-temperature thermoelectric materials, have been obtained by electrodeposition without the need for complexing the Sb cations in solution or further thermal treatment after deposition. The process consists of reduction of $\text{Bi}_{1-x}\text{Sb}_x$ directly from a solution of $\text{Bi}(\text{NO}_3)_3 \cdot 5\text{H}_2\text{O}$ and SbCl_3 in dimethyl sulfoxide at 25 °C on Pt electrodes. The electrodeposited films are polycrystalline and single phase under slow growth conditions, but two phases are observed under rapid growth conditions (more negative potentials) and for films with roughly equal amounts of Bi and Sb. 200-nm wire arrays of $\text{Bi}_{1-x}\text{Sb}_x$ were grown under similar conditions using porous alumina as a template. Arrays of dense, continuous, and highly crystalline $\text{Bi}_{0.84}\text{Sb}_{0.16}$ wires (close to the predicted optimum composition for thermoelectric applications) have been fabricated successfully at deposition potentials of -0.28 V vs Ag/AgCl from a solution of 0.050 M Bi and 0.030 M Sb in DMSO.

Introduction

There has been ongoing interest in developing thermoelectric devices for widespread use in refrigeration and power generation for the last forty years. Unfortunately, despite intense efforts, the efficiencies of thermoelectric devices have fallen short of those achieved with conventional refrigeration and power generation technologies. In recent years there has been a resurgence of interest in thermoelectric technologies because new experimental and theoretical results suggest that the thermoelectric efficiencies of quantum-confined materials are enhanced compared with those of bulk materials.^{1–4} For this reason, our group has been interested in the fabrication of nanowires of thermoelectric materials.

We have begun studies on the fabrication of $\text{Bi}_{1-x}\text{Sb}_x$ nanowires. $\text{Bi}_{1-x}\text{Sb}_x$ alloys are among the best low-temperature thermoelectric materials in bulk form. The maximum thermoelectric efficiency (ZT) is found at 80 K for alloys with 12% Sb (ZT = 0.88).^{5–7,10} In recent

theoretical work, Dresselhaus et al. predicted enhancements in ZT for $\text{Bi}_{1-x}\text{Sb}_x$ nanowires with diameters of 35–50 nm.⁷ Our strategy is to fill the high density of pores in porous alumina with $\text{Bi}_{1-x}\text{Sb}_x$ nanowires by electrodeposition.^{8,9} By the nature of electrodeposition, the wires will grow continuously. Moreover, with electrodeposition we can control the wire composition by manipulating various deposition conditions such as deposition potential and bath composition.

The first step in the electrodeposition of nanowires is to determine the appropriate conditions for the deposition of high-quality thin films, and then to use those optimized conditions as a starting point for filling the templates. Because $\text{Bi}_{1-x}\text{Sb}_x$ is an alloy, we need to find the optimal conditions that allow for the deposition of $\text{Bi}_{1-x}\text{Sb}_x$ with the right composition. Prior work has shown that $\text{Bi}_{1-x}\text{Sb}_x$ films can be electrodeposited if a means is found to overcome the low solubility of Sb salts.^{11–14} Besse et al.¹¹ have used potentiostatic depositions and complexed the cations in solution with a very

* To whom correspondence should be addressed via e-mail: msmg@ole.com. Current address: Instituto de Microelectrónica de Madrid, IMM (CNM-CSIC) C/Isaac Newton, 8 (PTM) 28760, Tres Cantos, Madrid, Spain.

[†] Department of Chemistry.

[‡] Department of Materials Science and Engineering.

[§] Current address: Department of Chemistry and Chemical Biology, Harvard University, 12 Oxford Street, Cambridge, MA 02138.

^{||} Current address: School of Materials Engineering, School of Electrical and Computer Engineering, and the Boirck Nanotechnology Center, Purdue University, 501 Northwestern Avenue, West Lafayette, IN 47907-2036.

(1) Hicks, L. D.; Harman, T. C.; Dresselhaus, M. S. *Appl. Phys. Lett.* **1993**, *63*, 3230–3232.

(2) Hicks, L. D.; Dresselhaus, M. S. *Phys. Rev. B: Condens. Matter* **1993**, *47*, 16631–16634.

(3) Hicks, L. D.; Dresselhaus, M. S. *Phys. Rev. B: Condens. Matter* **1993**, *47*, 12727–12731.

(4) Hicks, L. D.; Harman, T. C.; Sun, X.; Dresselhaus, M. S. *Phys. Rev. B: Condens. Matter* **1996**, *53*, 10493–10496.

(5) Cho, S. L.; DiVenere, A.; Wong, G. K.; Ketterson, J. B.; Meyer, J. R. *J. Vac. Sci. Technol., A* **1999**, *17*, 9–13.

(6) Lenoir, B.; Scherrer, H.; Caillat, T. *Recent Trends Thermoelectric Mater. Res. I Semiconductors and Semimetals* **2001**, *69*, 101–137.

(7) Rabin, O.; Lin, Y.-M.; Dresselhaus, M. S. *Appl. Phys. Lett.* **2001**, *79*, 81.

(8) Prieto, A. L.; Sander, M. S.; Martín-González, M. S.; Gronsky, R.; Sands, T.; Stacy A. M. *J. Am. Chem. Soc.* **2001**, *123*, 7160.

(9) (a) Sapp, S. A.; Lakshmi, B. B.; Martin, C. R. *Adv. Mater.* **1999**, *11*, 402. (b) Martin, C. R. *Science* **1994**, *266*, 1961.

(10) Cho, S.; DiVenere, A.; Wong, G. K.; Ketterson, J. B.; Meyer, J. R. *Phys. Rev. B: Condens. Matter* **1999**, *59*, 10691–10696.

(11) Besse, F.; Boulanger, C.; Lecuire, J. M. *J. Appl. Electrochem.* **2000**, *30*, 385–392.

(12) Shibleva, T. G.; Povetkin, V. V.; Zakharov, M. S. *Prot. Met. USSR* **1989**, *25*, 373–374.

(13) Povetkin, V. V.; Shibleva, T. G.; Kovenskii, I. M. *Sov. Electrochem.* **1990**, *26*, 1438–1441.

(14) Shibleva, T. G.; Povetkin, V. V.; Zakharov, M. S. *J. Appl. Chem. USSR JAPUAW* **1986**, *59*, 551.

(15) Martín-González, M. S.; Prieto, A. L.; Gronsky, R.; Sands, T.; Stacy A. M. *J. Electrochem. Soc.* **2002**, *149*, C546–C554.

high concentration of Cl^- (5 M), whereas Shibleva et al.^{12–14} used galvanostatic depositions in the presence of ethylenediaminetetracetic acid (EDTA or Trilon B) as the complexing agent. In both cases, the complexing agents increased the solubility of Sb salts in water. In this paper, we have studied the formation of $\text{Bi}_{1-x}\text{Sb}_x$ films and wires by electrodeposition from dimethyl sulfoxide (DMSO)² solutions containing Sb^{3+} and Bi^{3+} cations. DMSO was chosen as an alternative to water because of the higher solubility of Sb salts in DMSO than in water. Moreover, in DMSO more negative potentials can be used for film deposition without reduction of the solvent. Several Sb and Bi salts are readily soluble in DMSO, so there is a wide choice of starting materials.

Here we report the effects of various electrodeposition conditions (potential, concentration of the cations in solution, electrodes) on the synthesis of $\text{Bi}_{1-x}\text{Sb}_x$ films with a range of compositions. In addition, we report the electrodeposition of 200-nm $\text{Bi}_{1-x}\text{Sb}_x$ nanowires using porous alumina as a template. The conditions employed for the deposition of thin films were used as a starting point and then optimized to obtain wire arrays with composition close to 15% Sb (the composition predicted to yield the maximum ZT form p-type wires by Dresselhaus et al.). The composition and crystallinity of the as-deposited films and nanowire arrays were determined by powder X-ray diffraction, scanning electron microscopy, energy dispersive spectroscopy, and electron microprobe analysis.

Experimental Section

Note: For safety reasons gloves should be worn when using DMSO.

The solutions used for cyclic voltammetry experiments, film deposition, and nanowire depositions were prepared by dissolving $\text{Bi}(\text{NO}_3)_3 \cdot 5\text{H}_2\text{O}$ (Sigma Chemicals, 99.97%) and SbCl_3 (Sigma, 99.97%) in DMSO (Fisher, 99.9%). For cyclic voltammetry experiments solutions of Bi^{3+} (0.040 M $\text{Bi}(\text{NO}_3)_3 \cdot 5\text{H}_2\text{O}$), Sb^{3+} (0.040 M SbCl_3), and both together were studied. Films were deposited from three different solutions: (a) 0.020 M Bi^{3+} and 0.060 M Sb^{3+} ; (b) 0.040 M Bi^{3+} and 0.040 M Sb^{3+} ; and (c) 0.060 M Bi^{3+} and 0.020 M Sb^{3+} . These three solutions will be referred to as having Bi/Sb ratios of 3:1, 1:1, and 1:3, respectively. Nanowires were deposited from two different solutions: (a) 0.060 M Bi^{3+} and 0.020 M Sb^{3+} and (b) 0.050 M Bi^{3+} and 0.030 M Sb^{3+} , referred to with the Bi/Sb ratios of 3:1 and 5:3, respectively. In all solutions with mixtures of Bi and Sb, the total cation concentration is maintained at 0.080 M. A conventional three-electrode cell was used for the electrodepositions. All glassware was cleaned in a base bath and thoroughly washed with doubly distilled water.

The mechanism of the electrodeposition of $\text{Bi}_{1-x}\text{Sb}_x$ was studied by cyclic voltammetry using a Bioanalytical Systems Basomatic CV50W. This study was carried out under the same conditions as described in ref 15.

The electrodeposition of films was performed potentiostatically as was done in a previous work.¹⁵ The counter electrode was Pt gauze attached to a Pt wire and the reference electrode was Ag/AgCl (3 M NaCl, 0.175 V vs NHE). Several deposition potentials from -0.25 V to -1.52 V vs Ag/AgCl (3 M NaCl) and several solution concentrations were examined as well as several working electrodes (Ag, Ni, Au/Pd, and Pt). The volume of the bath was 50 mL and the temperature was 25 °C for all depositions. Slow stirring was used during deposition of films and 200-nm wires.

The electrodeposition of 200-nm wires was performed under similar conditions. The working electrode was a 1-cm diam. porous alumina filter with 60 μm long and 200-nm diam. pores (obtained from Whatman). A 1- μm -thick Pt layer was sputter-

deposited on one side (RANDEX, Perkin-Elmer model 2400). The alumina template was then glued to a Cu disk with Ag paint and allowed to dry for several hours. The back of the Cu disk was soldered to a Cu wire, and painted with an insulating epoxy (Rector Seal) to ensure that deposition could occur only at the base of the pores. This working electrode assembly was then air-dried for at least 12 h. The counter electrode and the reference electrode were the same as those used for films. The volume of the bath was 50 mL and the temperature was 25 °C for all depositions.

X-ray diffraction (XRD) patterns of the films and wire arrays were obtained using a Siemens D5000 diffractometer. The lattice parameters were calculated by studying the displacement of the maxima in the diffraction pattern using the substrate (Pt) as an internal standard.

The compositions of the films were determined by electron microprobe analysis (EPMA, Cameca SX-51). The film samples were mounted on glass slides with epoxy and coated with carbon. The microanalyses were performed on 50 different points across the sample. Antimony (99.999%) and bismuth (99.9999%) standards were used to calibrate the data. The results presented in this paper are the average over the sites measured, excluding sites within ~ 2 mm of the edges of the electrodes. Films grown at less negative potentials were smooth and had standard deviations as low as 0.26 atomic %. However, the standard deviations for films grown at more negative potentials were as high as 8%, presumably due to increased roughness and decreased homogeneity.

Scanning electron microscopy (SEM, Hitachi S-5000) was carried out to determine the morphology of the electrodeposited thin films and the 200-nm wire arrays. Energy-dispersive spectroscopy (EDS, JEOL 6300) was used to estimate the chemical composition of the 200-nm wire arrays. SEM and EDS were performed on the wires by cleaving a filled template, and analyzing the sample edge-on. In a typical EDS measurement, the composition was measured on 10 points along the length of the cross section of the template. The standard deviations of the measurements were within 3 atomic %, which is typical for samples with surface roughness.

Results and Discussion

In previous electrochemical studies of the deposition of $\text{Bi}_{1-x}\text{Sb}_x$ films, 1 M HCl was used as a solvent. In addition, a high concentration of NaCl (4 M)¹¹ or EDTA^{12–14} was necessary to form the chloro or EDTA complexes of Sb^{3+} and Bi^{3+} to promote dissolution. However, even under these conditions, Sb^{3+} is not very soluble. This limits the ability to tune the solution concentrations, which we will show is key in determining the composition of the electrodeposited films. The advantage of DMSO as a solvent is that a higher concentration of Sb can be reached by dissolution of SbCl_3 . In addition, DMSO has a much larger solvent window than water, which allows for the use of a wider range of potentials to tune the film properties without reduction of the solvent.

We have studied the electrochemical behavior of both cations in DMSO. Following the identification of reduction potentials that lead to film formation by cyclic voltammetry, films were deposited from solutions with three different compositions. Finally, 200-nm wire arrays were prepared by deposition into porous alumina templates. These three sets of experiments are described below.

Cyclic Voltammetry. The cyclic voltammogram for both cations together in DMSO is shown in Figure 1. A single very broad reduction wave is observed with $E_{\text{pc}} \sim -0.65$ V, labeled peak A, instead of two different waves corresponding with each cation. This reduction wave can be attributed to the direct deposition of the

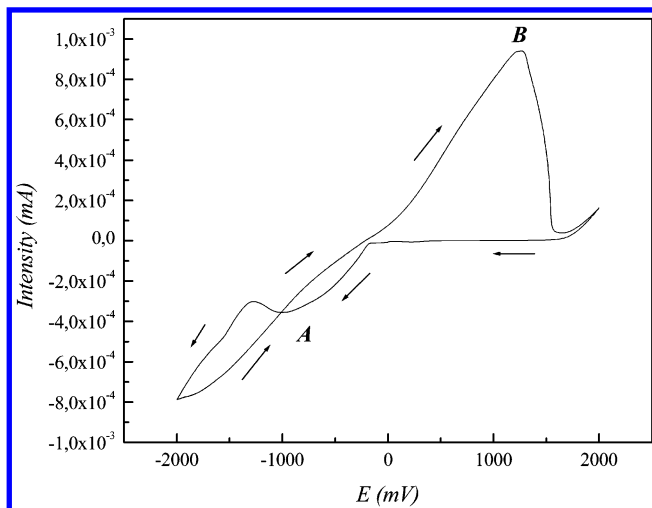
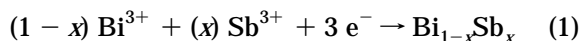


Figure 1. Cyclic voltammetry of 0.040 M Bi^{3+} - $\text{Bi}(\text{NO}_3)_3 \cdot 5\text{H}_2\text{O}$ - plus 0.040 M Sb^{3+} - SbCl_3 . Scan rate, 0.01 V/s^{-1} ; reference electrode, Ag/AgCl (3 M NaCl); temperature, 25 °C.

$\text{Bi}_{1-x}\text{Sb}_x$ solid solution according to the following reaction.



The observation of a single oxidation peak at $E_{\text{pa}} = \sim 0.45$ V vs Ag/AgCl , labeled Peak B, could be due to two different possibilities: (a) the presence of domains of individual elements, one under the other, so that during the oxidation the top layer has to be oxidized first before removing the under layer; or (b) the formation of a solid solution rather than co-deposition of the metals, because a heterogeneous mixture of the two elemental metals would give two oxidation waves corresponding to the independent dissolution of each metal. As will be discussed below, the formation of $\text{Bi}_{1-x}\text{Sb}_x$ as opposed to the deposition of Bi and Sb layers is confirmed by XRD, as all the diffraction maxima can be indexed with a single phase for films. This confirms that Reaction 1 is the process related to the electrodeposition of Bi and Sb in DMSO. This assignment is in good agreement with what has been reported regarding aqueous solutions.¹⁶

$\text{Bi}_{1-x}\text{Sb}_x$ Films. Before investigation of the composition and morphology of the $\text{Bi}_{1-x}\text{Sb}_x$ films could begin, we needed to find a suitable substrate (working electrode). From the CV and XRD studies, it was evident that Bi, Sb, and $\text{Bi}_{1-x}\text{Sb}_x$ formed stable films on Pt. Although several other electrode materials were subsequently tested (Ag, Ni, and Au/Pd), adhesion of the electrodeposited films and film quality were found to be the best on Pt electrodes, as detected by SEM. Because of the higher quality of the films deposited on Pt as opposed to those deposited on the other substrates, Pt electrodes were used for all of the film studies presented in this paper.

Alloys of $\text{Bi}_{1-x}\text{Sb}_x$ of varying composition were deposited potentiostatically from solutions of $\text{Bi}(\text{NO}_3)_3 \cdot 5\text{H}_2\text{O}$ and SbCl_3 in DMSO at 25 °C. Two main electrodeposition parameters were studied: (1) potential and (2) relative concentrations of the cations in solution.

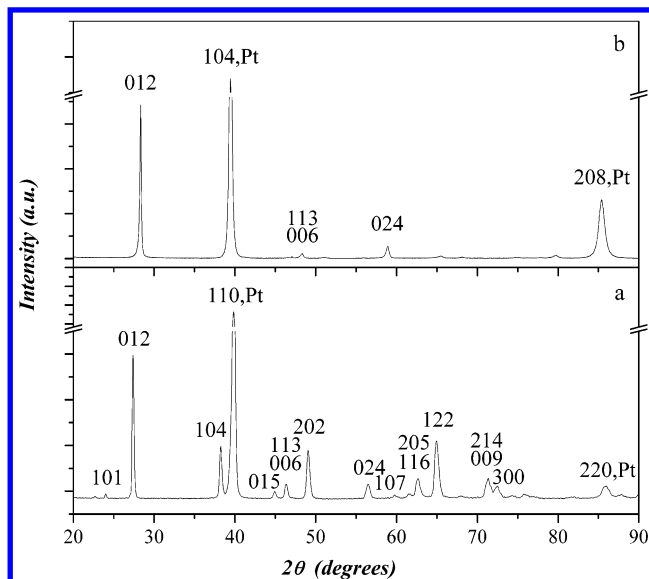


Figure 2. XRD patterns of two $\text{Bi}_{1-x}\text{Sb}_x$ films. The films were obtained from two solutions: (a) 0.02 M Bi^{3+} plus 0.06 M Sb^{3+} ; and (b) 0.06 M Bi^{3+} plus 0.02 M Sb^{3+} . The depositions were carried out at $E = -1.02$ V vs Ag/AgCl (3 M NaCl) for 1 h. The film compositions are $\text{Bi}_{0.95}\text{Sb}_{0.05}$ and $\text{Bi}_{0.10}\text{Sb}_{0.90}$, respectively, as determined by EPMA.

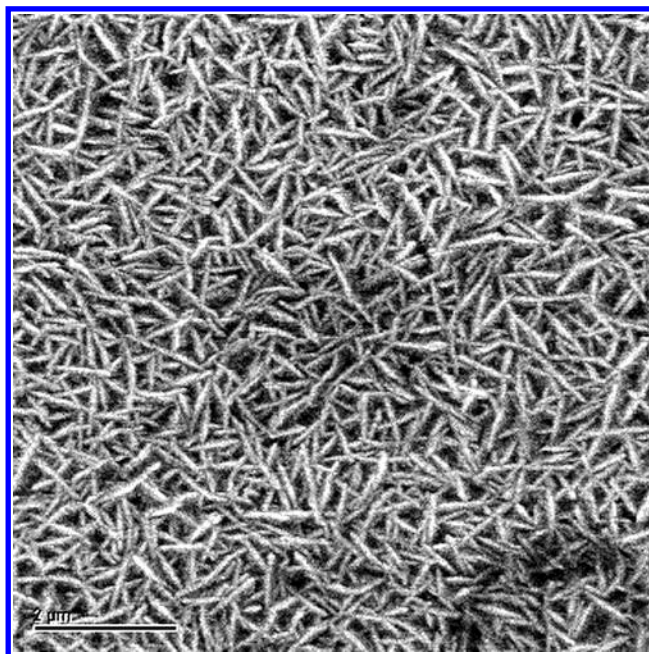


Figure 3. SEM micrograph of a film with composition $\text{Bi}_{0.10}\text{Sb}_{0.90}$. The features are characteristic of all the films deposited at -1.02 V vs Ag/AgCl (3 M NaCl) for 1 h.

For Bi/Sb ratios of 1:3 in solution, films were deposited at potentials of -1.02 V and -1.52 V vs Ag/AgCl . For both deposition potentials, the films were approximately 10% Bi and 90% Sb as determined by EPMA. These values were consistent at more than 50 locations across the film (excluding regions within 2 mm of the edges), indicating that the films are relatively homogeneous. The peaks in the XRD patterns were sharp and narrow, indicating that the films are highly crystalline and consist of only one phase (Figure 2a). The peaks are slightly shifted to larger d spacing as compared with those of pure Sb, which is consistent with the formation of a solid solution. As can be seen in the

(16) Sutkus, A.; Tolutis, R. *Phys. Status Solidi A* **1999**, *173*, 417-424.

Table 1. Atomic Percentages of Bi/Sb in Films Electrodeposited on Pt Electrodes as a Function of Bi and Sb Concentration^a

solution concentration Bi:Sb (M)	composition by EPMA Bi:Sb (%)	alloy formula	<i>c</i> parameter from XRD (Å)	<i>a</i> parameter from XRD (Å)	composition <i>a</i> parameter XRD
	0:100	Sb	11.274(6) ¹⁷	4.3084(2) ¹⁷	100% Sb
0.02:0.06	10(1):90(1)	Bi _{0.10} Sb _{0.90}	11.345(1)	4.33(1)	89(1)% Sb
0.04:0.04	52(5):48(5)	Bi _{0.52} Sb _{0.48}	2-phase mixture	2-phase mixture	
0.06:0.02	95(2):4(2)	Bi _{0.95} Sb _{0.05}	11.852(1)	4.54(1)	4.5(0.1)% Sb
	100:0	Bi	11.862(6) ¹⁷	4.5460(5) ¹⁷	100% Bi

^a Solutions were prepared by dissolving Bi(NO₃)₃·5H₂O and SbCl₃ in DMSO, and the depositions were carried out at -1.02 V vs Ag/AgCl (3 M NaCl) for 1 h at 25 °C. The percentages of Bi and Sb were determined by EPMA and from the *a* lattice parameter using Berger's formula.¹⁷

SEM image shown in Figure 3, films grown at -1.02 V are smooth with a relatively small grain size (~600 × 80 nm).

For Bi/Sb ratios of 1:1 in solution and deposition potentials of -1.02 V and -1.52 V vs Ag/AgCl, the films produced were roughly 50% Bi and 50% Sb as determined by EPMA. As the electron probe was scanned across the film, these numbers fluctuated by ±15% indicating that the films are not as homogeneous as the Sb-rich films. Although the deposition potential had little effect on the overall film composition, the XRD patterns for each sample were markedly different. At the more negative potential, -1.52 V, there were two sets of peaks near those of both pure Sb and pure Bi, indicating the co-deposition of two phases (one Bi-rich and the other one Sb-rich). In contrast, the XRD patterns for the films deposited at -1.02 V show only a single alloy phase with peaks between those of pure Sb and pure Bi (albeit broader than those for the Sb-rich films). The films prepared at the more negative potential were also quite rough as determined by SEM, indicative of rapid growth. We conclude that single alloy films with roughly equal amounts of both Sb and Bi can be obtained for potentials that are not overly negative. At very negative potentials, rapid growth leads to co-deposition of two phases with different compositions as opposed to one solid solution.

For Bi/Sb ratios of 3:1 in solution, a composition in the range of interest for thermoelectric applications was expected. Therefore, a wider range of potentials was tested from -0.27 to -1.52 V vs Ag/AgCl to determine in more detail the range of compositions accessible. The films produced were all Bi-rich, with roughly 95% Bi and 5% Sb. The peaks in the XRD patterns were all relatively narrow, indicating a high degree of crystallinity, and only one compositional phase was observed (Figure 2b). The peaks are slightly shifted to smaller *d* spacing as compared with those of pure Bi, which is consistent with the formation of a solid solution. The dominant crystalline orientation depends on the chemical composition. SEM images of the Bi-rich films are in Figure 3 with an average crystallite size of 1 × 0.1 μm.

XRD patterns were further analyzed to obtain information about the correlation of lattice parameters with composition. As expected for a solid solution, there is a shift toward larger angles in 2θ with an increase in Sb concentration. The lattice parameters obtained using Pt as an internal standard are given in Table 1. There is a systematic decrease in both *a* and *c* parameters with increasing Sb content, consistent with the expected decrease in cell volume. Berger et al.¹⁷ determined a correlation between cell parameters and the value of *x*

in Bi_{1-x}Sb_x alloys:

$$a = (0.454469 \pm 0.00044) - (0.02398 \pm 0.00072)x$$

$$c = 1.186294 - [0.058632/(1 + ((1.260 \pm 0.043)*(1/x - 1)))]$$

Those compositions calculated using Berger's correlation and the values of *a* as determined from XRD are in good agreement with the relative concentrations as determined by EPMA (see Table 1).

We conclude that the films prepared by electrodeposition are a solid solution, and not a physical mixture of Bi and Sb, with the exception of films of roughly equal amounts of Bi and Sb and films that are grown too rapidly (at more negative potentials). The compositions of the films are strongly correlated with the relative concentrations of the Bi and Sb in solution, and less dependent on other factors such as the potential and the deposition time. Compositions obtained under slow growth conditions for different electrolyte compositions are compared in Table 1. The composition of the films becomes more Bi-rich as the ratio of Bi/Sb is increased. Both Sb-rich and Bi-rich films prepared at the same potential show similar morphology. A representative example can be found in Figure 3. The dependence of the ratio of Bi/Sb in solution to the composition of Bi and Sb in the deposited solid solution is in good agreement with what has been observed for alloys deposited from aqueous solutions.¹¹⁻¹⁴

200-nm Bi_{1-x}Sb_x Wires. Arrays of Bi_{1-x}Sb_x nanowires with 200 nm diameters were fabricated by electrodeposition into porous alumina to determine whether high-quality nanowires could be made. We started with the conditions used for the films, and then tuned the parameters to get better wires. DMSO solutions with Bi/Sb ratios of 3:1 and 5:3 were used. Because slow growth conditions lead to more highly crystalline nanowires and a higher degree of pore filling, less negative potentials were used for nanowire growth: -0.52 V and -0.28 V vs Ag/AgCl.

Depositions performed at -0.52 V vs Ag/AgCl with a Bi/Sb ratio of 3:1 produced wires that were 7% Sb and 93% Bi as determined by EDS along the cross-section of the template. The XRD pattern of this sample indicates that polycrystalline wires are obtained, with a slight co-deposition of Sb, as indicated by the presence of a small Sb₀₁₂ peak (Figure 4). This peak does not have any displacement with respect to the PDF file. This Sb

(17) Berger, H.; Christ, B.; Troschke, J. *Cryst. Res. Technol.* **1982**, *17*, 1233.

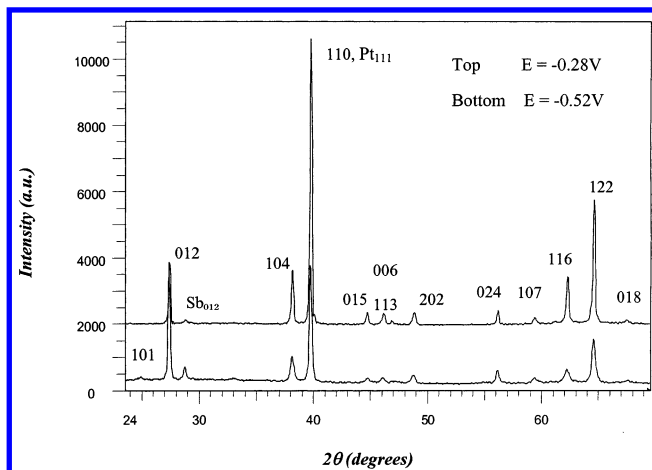


Figure 4. XRD patterns of 200-nm Bi/Sb wire arrays deposited at $E = -0.52$ V and -0.28 V vs Ag/AgCl from a bath of 0.06 M Bi and 0.02 M Sb. The Miller indices indicate the alloy peaks. The peak widths are narrower for the slower growth conditions ($E = -0.28$ V), indicating a more homogeneous sample.

peak was not found for films. By using slower growth conditions ($E = -0.28$ V), a sample that exhibits narrower peak widths in the XRD is obtained, indicating a more homogeneous sample. The composition of the wires remained the same within the error of the measurement. The $\text{Sb}_{0.12}$ peak seems, a priori, to be lower in intensity relative to the alloy peaks, for -0.28 V, which can be due to a lesser amount of Sb in the deposit or more probably to a change in the relative intensity of the diffraction peak due to an increase in the homogeneity and the orientation of the wires. This is also in agreement with the narrower peaks observed for the alloy films. We conclude that the Bi-rich phase that forms at -0.28 V is reasonably homogeneous, indicating that the wires are more homogeneous for slower growth rates.

The presence of essentially pure Sb is intriguing. If the second phase were due to phase separation, we would expect an Sb-rich phase, not pure Sb. When the Pt and the bottom $1\text{--}2\ \mu\text{m}$ of template were removed by mechanical polishing the XRD pattern showed no evidence of the $\text{Sb}_{0.12}$ peak. Therefore, we can conclude that the pure Sb seems to be deposited in the first stages of the electrodeposition process for deposition into porous alumina, followed by the deposition of $\text{Bi}_{1-x}\text{Sb}_x$ alloy.

The observation of the initial deposition of Sb followed by the deposition of Bi-rich alloys suggests two main deposition stages. In the early stages, the electrodeposition is governed by formation of the double layer, adsorption phenomena, equilibrium between cations, surface characteristics of the electrode, and/or molecular-scale events, etc. These processes affect the relative concentration of Bi and Sb within the pores near the electrode differently compared with the relative concentrations in the bulk solution. On the basis of our results, we conclude that the conditions in the early stages seem to favor either the deposition of pure Sb or the co-deposition of $\text{Bi}_{1-x}\text{Sb}_x$ and Sb. Once steady state conditions are reached, the main process that governs the relative concentration of the cations is the mass transport from the bulk toward the surface of the

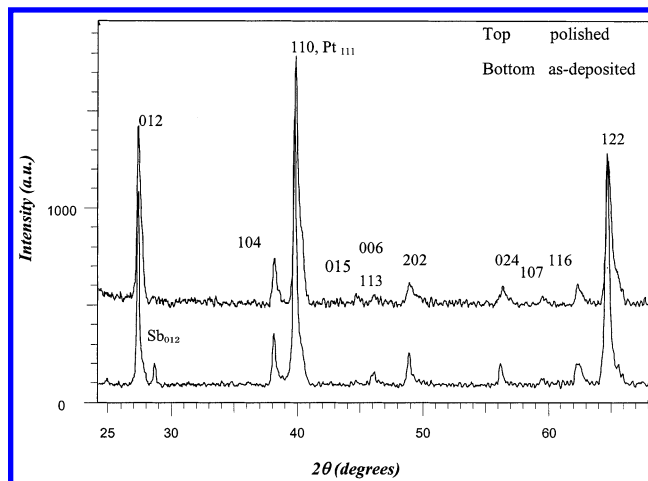


Figure 5. XRD pattern of 200-nm Bi/Sb wire array grown at $E = -0.28$ V vs Ag/AgCl from a bath of 0.05 M Bi and 0.03 M Sb. EDS shows that the average composition of the wires is $\text{Bi}_{0.86}\text{Sb}_{0.14}$. Once the Pt substrate and $\sim 1\ \mu\text{m}$ of the bottom of the wires has been removed, the peaks associated with Sb disappear. Note that the shoulders on the peaks indicate a small degree of inhomogeneity. Also, the high intensity of the 110 peak relative to the 012 peak indicates that the wire texture is [110].

nano-electrodes. During this stage, we observed the deposition of Bi-rich alloy wires, which are reasonably homogeneous.

To obtain wires with a higher Sb composition, depositions were performed at -0.28 V vs Ag/AgCl, but with a Bi/Sb ratio of 5:3 (relatively richer in Sb). With this bath composition, the wire composition was richer in Sb, 14% Sb and 86% Bi, as determined by EDS. This composition is in the range of interest for predicted enhancements in thermoelectric efficiency. The peaks in the XRD pattern are narrow (although shoulders can be observed in some of the peaks indicating a range of compositions) and shifted toward higher 2θ as expected (Figure 5). The high intensity of the 110 peak relative to the 012 peak indicates that the wire texture is [110]. The $\text{Sb}_{0.12}$ peak is still observed, which indicates that there is still a preferential deposition of Sb at the bottom of the pores due to processes related to the initial stages of the electrodeposition.

SEM images of the bottom of the template after removal of the electrode material (Pt) by mechanical polishing (Figure 6a) show that nucleation occurs in greater than 95% of the pores. This is important because a high wire density is required for thermoelectric applications. Images of the cross-section, Figure 6b, of the templates show that the wires are dense and continuous. Small gaps can be found between the template and some of the wires, marked with an arrow. Nonwetting effects between the alumina and the $\text{Bi}_{1-x}\text{Sb}_x$ solid solution could explain this behavior. Similar behavior has been observed for both 200-nm and 40-nm $\text{Bi}_{2-x}\text{Sb}_x\text{Te}_3$ ¹⁸ and 40-nm $\text{Bi}_{1-x}\text{Sb}_x$,¹⁹ but not Bi_2Te_3 ⁸ or Bi^{20} in porous alumina. Moreover, different

(18) Martín-González, M. S.; Prieto, A. L.; Gronsky, R.; Sands, T.; Stacy, A. M. *Adv. Mater.* **2003**, in press.

(19) Prieto, A. L.; Martín-González, M. S.; Gronsky, R.; Sands, T.; Stacy, A. M. *J. Am. Chem. Soc.* **2003**, *125*, 2388–2389.

(20) Yin, A. J.; Li, J.; Jian, W.; Bennett, A. J.; Xu, J. M. *Appl. Phys. Lett.* **2001**, *79*, 1039.

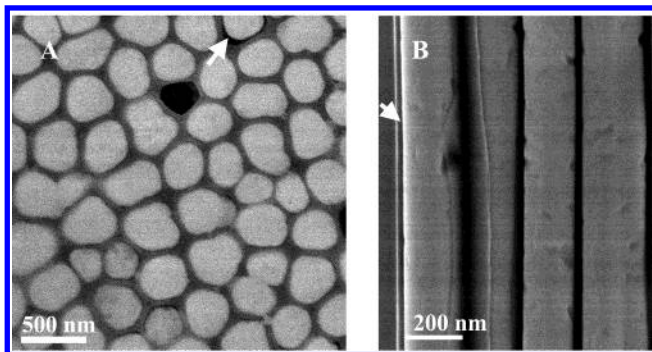


Figure 6. SEM nanowires of $\text{Bi}_{0.85}\text{Sb}_{0.15}$ nanowires: (a) bottom view after removal of the Pt electrode by mechanical polishing; and (b) cross-section or edge view. The lighter regions are the wires. They are dense. The filling of each pore is very high, yet does not completely fill the pores in all regions (gap marked with an arrow). Nucleation and growth of wires occurs in greater than 95% of the pores.

solvents (water and DMSO) have also been used for $\text{Bi}_{2-x}\text{Sb}_x\text{Te}_3$ and $\text{Bi}_{1-x}\text{Sb}_x$, respectively.

Conclusions

Films and 200-nm wire arrays of $\text{Bi}_{1-x}\text{Sb}_x$ solid solutions can be electrodeposited directly by a three-electron reduction from solutions of Bi^{3+} and Sb^{3+} in DMSO without further thermal treatment or the need for complexing the Sb^{3+} in solution. Under slow growth conditions and a relative concentration of Bi/Sb of 1:3

and 3:1, the films deposited are smooth, single-phase (Sb-rich and Bi-rich, respectively), and crystalline. Codeposition can be observed for films grown from solutions with roughly equal amounts of Sb and Bi under rapid growth conditions. Arrays with 200-nm $\text{Bi}_{0.84}\text{Sb}_{0.16}$ wires can be obtained at room temperature from a solution with a Bi/Sb ratio of 5:3 in DMSO and a potential of -0.28 V vs Ag/AgCl. The wires are dense and continuous, and they almost completely fill the pores.

Acknowledgment. This work was funded by the Office of Naval Research (ONR N00014-01-1-1058). Additional support was provided by the Department of Defense ONR-MURI on Thermoelectrics, N00014-97-1-0516. We thank Margaret Chan and Andrea Kops for their help in the fabrication of the films, Jenny Keyani for her help in the fabrication of the 200-nm nanowires, Professor Jeffrey Long and his group for the use of the Bioanalytical Systems Basomatic CV50W, Dr. Gordon Vrdoljak for help with the SEM (Electron Microscope Lab, UCB), John Donovan for help with the EPMA (Electron Probe Microanalysis Laboratory, UCB), and Ron Wilson for help with the SEM/EDS system (Department of Materials Science and Engineering). M.S.M.G thanks the MEC/Fulbright Postdoctoral Fellowship program and A.L.P. thanks Lucent Technologies, Bell Labs for funding.

CM021027F